sustainability

MDPI

Article

Investigation of Coupling Effects of Wave, Current, and Wind on a Pile Foundation

Zhibin Tu [1,*], Jianfeng Yao [1], Mingfeng Huang [2] and Wenjuan Lou [2]

[1] College of Civil Engineering and Architecture, Zhejiang University of Water Resources and Electric Power, Hangzhou 310018, China
[2] College of Civil Engineering and Architecture, Zhejiang University, Hangzhou 310058, China
* Correspondence: tuzb@zju.edu.cn; Tel.: +86-0571-86929012

Abstract: To investigate the coupling effects of wave–wind, wave–current, and wave–current–wind on a pile foundation of a marine structure, harbor basin tests on loads induced by single and combined action of wave, current, and wind were conducted. The time histories, power spectrums, and characteristic values of drag forces in the test conditions were compared. Then, the coupling coefficients were calculated based on the characteristic values to quantitively evaluate the coupling effects. The influence of natural vibration of the pile on the characteristic values and coupling effects were studied by comparing the test loads between rigid and elastic models. The results show that the shapes of power spectrums of drag forces and their peak frequencies in the wave-involved conditions are similar to the spectrum of incident wave, which means that the steady current and uniform wind cannot change the frequency distribution of incident random wave. Although the drag forces of rigid and elastic model under wave–wind, wave–current, and wave–current–wind are not the linear superposition of corresponding single field, the coupling effects among them are quite weak as the coupling coefficients are small. It is speculated that the weak wave–wind coupling effect may be because, firstly, the interaction of wave and wind is limited to the zone near the water surface, which is far less than the height of the model; secondly, the wave-induced load is dominant compared to wind and current. The loads in test conditions of elastic model are similar to the rigid model; for that, the model's natural frequency is far away from the peak spectral frequency of incident wave, having little influence on the drag force.

Keywords: pile foundation; harbor basin test; wave–current–wind; coupling effects

check for updates

Citation: Tu, Z.; Yao, J.; Huang, M.; Lou, W. Investigation of Coupling Effects of Wave, Current, and Wind on a Pile Foundation. *Sustainability* **2022**, *14*, 14272. https://doi.org/10.3390/su142114272

Academic Editor: Byungik Chang

Received: 14 September 2022
Accepted: 28 October 2022
Published: 1 November 2022

Publisher's Note: MDPI stays neutral with regard to jurisdictional claims in published maps and institutional affiliations.

Copyright: © 2022 by the authors. Licensee MDPI, Basel, Switzerland. This article is an open access article distributed under the terms and conditions of the Creative Commons Attribution (CC BY) license (https://creativecommons.org/licenses/by/4.0/).

1. Introduction

Wave, current, and wind are the main environmental actions for marine structures [1–3]. Many studies reported the dynamic responses of marine structures under single action of wave, current, or wind [4–11], but studies have rarely reported the coupling effects of the combined action of the three fields [12–15].

In order to describe the interaction among wave, current, and circulation, and simulate the vertical distribution of the flow field, Zhang et al. [13] built a wave-current coupling system based on the MASNUM wave model and POM circulation model. It was found that the variation trend of wave height and direction was consistent with the spiral structure of tropical storms in the coupling system, but due to the asynchronous data transmission, the effect of interaction of wave and current might not be reproduced. To investigate the influence of current on significant wave height in the wave–current interaction, Liu et al. [14] constructed a wave–current coupling numerical model based on the ROMS and SWAN wave models, and found that the interaction between wave and current was an important reason for the strengthening of current. However, the coupling effects of wave and current on marine structures were not investigated in the above studies.

A physical model test in wind wave trough is an effective way to study the coupling effects of wind, wave, and current. Su [15] discussed a method to simulate the combined

wind and wave field in the wind wave trough and made random wave by artificial wind-generated waves. This study overcame the defect of insufficient length of wind area in the wind wave trough. However, unfortunately, the simulated wind field in the test was inaccurate. Liu [16] studied the characteristics of wind–wave-induced dynamic responses of the tower-foundation system of a cross sea bridge through a wind–wave tunnel test. It was found that the coupling effect of wind and wave was significant in the wave controlling area, enlarging the displacement of tower top, while the influence of wave could be ignored in the wind controlling area. Chen [17] carried out a similar study to Liu [16] to investigate the dynamic response characteristics of a tower-foundation system due to the coupling effects of wind and wave, and found that the load on the bottom of foundation was mainly induced by wave, while the displacement of bridge tower top was mainly induced by wind, the coupling effect of wave and wind on the system was little. Liu et al. [18] investigated the coupling effects of wave, current, and wind on a foundation in a harbor basin and found that in most cases, the loads induced by combined action of the three flow fields were a little larger than the linear superposition of loads induced by single field, but in some cases, the conclusion was opposite. It could be seen in the above studies that as the interaction among wave, current, and wind was quite complicated, their coupling effects on marine structures are not clear. However, some researchers believed that there was a certain extent of coupling effect among wind, wave, and current. Shang [19] investigated the drag force on piles induced by wave and current based on the SWAN+ADICIRC model and discovered that if considering the coupling effect of wave and current, the drag force would reduce by about 17.4%. Based on the JCSS combination model, Fang [20] found that the combined load dominated by wind was theoretically 20–30% larger than that dominated by wave and current.

Herein, to investigate the coupling effects of wave, wind, and current on a pile foundation, a harbor basin test on loads induced by the single and combined action of wave, current, and wind was conducted. Firstly, both rigid and elastic models of the pile were made, and the drag forces of the base were obtained under the single and combined action of wave, current, and wind. Then, the time histories, power spectrums, and characteristic value of drag force in each case were compared. The coupling coefficients were defined and calculated based on the characteristic values to quantitatively evaluate the coupling effects of wave–current, wave–wind, and wave–current–wind. The influence of natural vibration of the pile on the characteristic values and coupling effects was studied by comparing the test loads between rigid and elastic models. Finally, some useful conclusions about coupling effects of wave, wind, and current were drawn.

2. Harbor Basin Tests

2.1. Test Facilities

The model tests were conducted at the harbor basin of Tianjing Research Institute for Water Transport Engineering. The harbor basin is 45 m in length, 40 m in width, and 1.2 m in depth. Random wave, steady current, and uniform wind were generated in this study. Random wave was generated by a L-shaped multi-directional irregular wave generator, which is equipped on the long and short sides of the basin, as shown in Figure 1. A circulating steady current was made by 24 axial pumps and 4 diversion walls, as shown in Figure 2. The pumps were set downstream of the test area. A uniform wind field was made by a set of high-powered fans. As seen in Figure 2, the fan-set arranged on the pervious plate was at the upstream of the test area, consisting of 8 fans and covering the model testing area.

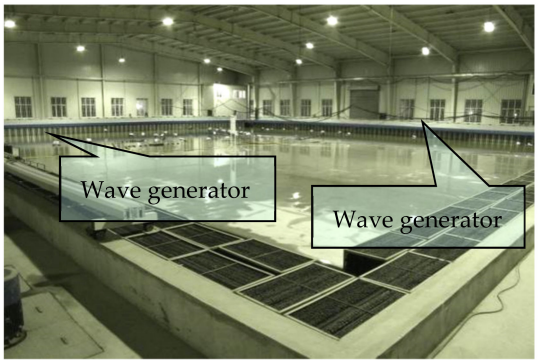


Figure 1. Harbor basin and its equipped L-shape multi-directional irregular wave generator.

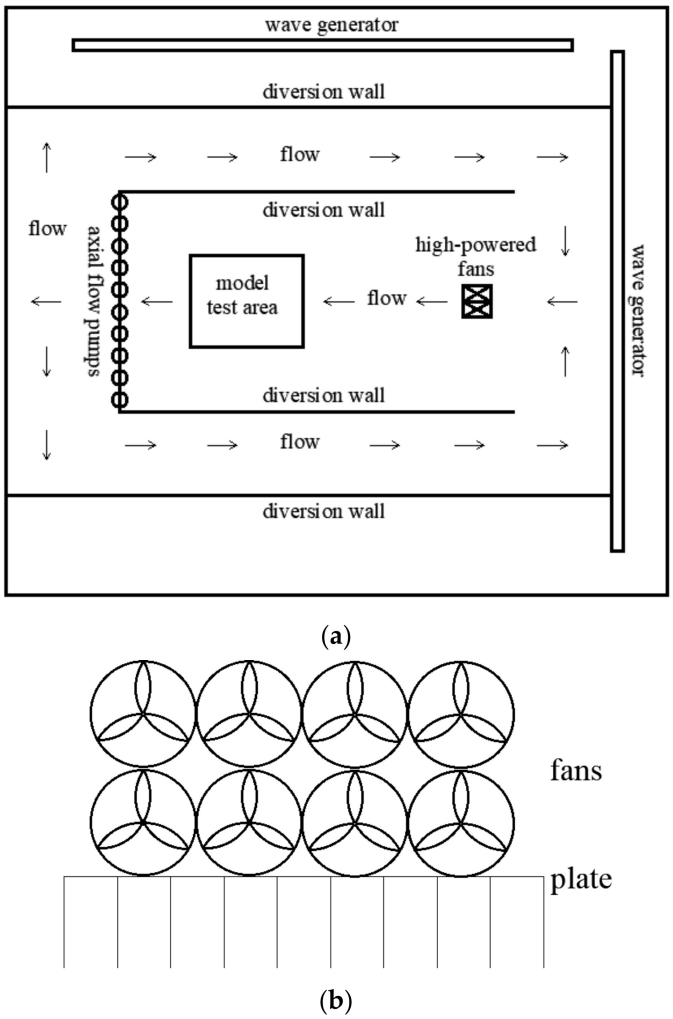


Figure 2. (**a**) Schematic diagram of steady current generation, and (**b**) the arrangement of high-powered fans.

The wave height was acquired by a TK-2008 wave height instrument. The water level was controlled by a M60 measuring needle. The current speed was controlled by the power of pumps and measured by a Vectrino current meter produced by Nortek Company in China. The wind speed was controlled by a frequency converter, with a maximum speed of 14 m/s, and measured by a hot-wire anemometer. The installation height of the anemometer was 10 m above the water surface in prototype, and had to converse to the model based on length scale ratio when tested.

2.2. Rigid Model

The test objective was a hollow pile foundation of a large offshore structure. The prototype of the pile was 6 m in outer diameter, 4 m in inner diameter, 120 m in height, and made of reinforced concrete. the length scale ratio of rigid model was 1:100, therefore the rigid model was 0.06 m in diameter and 1.2 m in height. To ensure the stiffness, the rigid model was made by solid steel column.

2.3. Elastic Model

According to the π-principle, the geometric, kinematic, and dynamic similarity should be satisfied in the elastic model. Geometric similarity is the basis similarity among them. To satisfy the three similarities, the criterion in Table 1 should be followed. The meaning and value of each ratio is listed in Table 2. As the Froude and Cauchy criterion cannot be satisfied at the same time, the elastic model was designed following the Froude Criterion, then the Cauchy and Euler criterion would be satisfied automatically, while the Reynolds Criterion was satisfied approximately.

Table 1. Similarity criterions followed by elastic model.

Similarity Criterions	Dimensionless Parameters	Expression
Froude Criterion	Gravity parameter	$\lambda_U^2/\lambda_l\lambda_g$
Cauchy Criterion	Elastic parameter	$\lambda_\rho\lambda_U^2/\lambda_E$
Euler Criterion	Pressure parameter	$\lambda_P/\lambda_\rho\lambda_U^2$
Reynolds Criterion	Viscosity parameter	$\lambda_l\lambda_U/\lambda_V$

Table 2. Meanings of ratios in similarity criterions.

Similarity Criterions	Dimensionless Parameters	Values
λ_l	geometric scale ratio	100
λ_U	velocity scale ratio	10
λ_g	density scale ratio	1
λ_P	Viscosity parameter	1
λ_E	modulus scale ratio	100
λ_P	pressure scale ratio	100
λ_V	scale ratio of fluid kinematic viscosity coefficient	1

The elastic modulus, density, and Poisson ratio of the prototype, which was made of reinforced concrete, were 3.15×10^4 MPa, 2.6×10^3 kg/m^3, and 0.3, respectively. The dynamic characteristics of the prototype were controlled by its first order modal, whose corresponding first order frequency was 0.244 Hz. Considering the similarity criterion, test condition, and material characteristics, the geometric scale ratio of the elastic model was 1:100, which is the same as rigid model. Then, the outer diameter, inner diameter, and height of the elastic model were 0.06 m, 0.04 m, and 1.2 m, respectively. The elastic modulus, density, Poisson ratio, and first order frequency of elastic model were 3.15×10^2 MPa, 2.6×10^3 kg/m^3, 0.3, and 2.439 Hz theoretically. To satisfy the above physical characteristics, the elastic model was made of special weighted rubber. The elastic modulus, density, and Poisson ratio of elastic model used in the test were 3.05×10^2 MPa, 2.54×10^3 kg/m^3, and 0.26, respectively.

A mold was made based on the geometric dimensions before making the elastic model. Then, the hot solution of special weighted rubber was poured into the mold. The first order frequency of elastic model is 2.326 Hz. As the error between elastic model and prototype is 4.6%, the elastic model design meets the requirements of the Chinese standard JTJ/T234-2001. The elastic model of the pile was displayed in Figure 3. Both rigid model and elastic model were fixed on the basin.

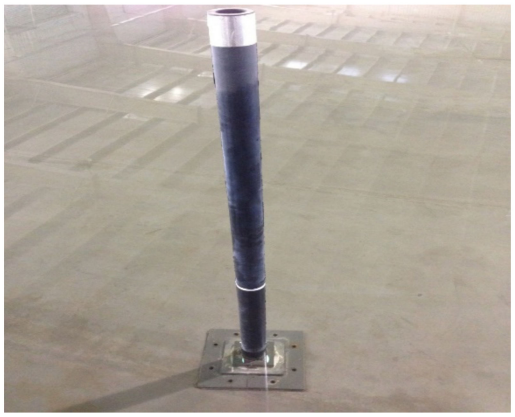


Figure 3. Elastic model of the pile.

2.4. Test Plans

The aim of this study was to explore the coupling effects of wave–wind, wave–current, and wave–current–wind through the drag forces of the rigid and elastic models under the single or combined actions of random wave, steady current, and uniform wind. The drag forces were recorded by an Underwater High Frequency Force Balance (UHFFB). To eliminate the influence of atmospheric and hydrostatic pressure, the UHFFB was calibrated to 0 in still water. When the geometric scale ratio λ_l = 100, the velocity scale ratio λ_U would be 10. The test conditions of rigid model are elaborated in Table 3, in which H_s, T_s, and γ_η represent the significant wave height, corresponding average period, and peak spectral factor random wave, V_c is the velocity of steady current, V_w is the speed of uniform wind. All parameters in Table 3 were converted to test model based on scale ratio. The simulated spectrum of incident random wave agreed with the JONSWAP random wave spectrum, with a corresponding peak spectral factor of 3.3. In the first 6 conditions, the random wave (G1~G2), steady current (G3~G4), and uniform wind (G5~G6) were produced, respectively. In G7~G10, both random wave and steady current were produced. In G11~G14, both random wave and uniform wind were produced. Finally, in G15~G22, three fields were produced together. Water depth in all conditions was 0.5 m. The test scene of rigid model is displayed in Figure 4.

Table 3. Test conditions of rigid model.

Conditions	Random Wave				Steady Current	Uniform Wind	Water Depth (cm)
	H_s (cm)	T_s (s)	Wave Spectrum	γ_η	V_c (cm/s)	V_w (cm/s)	
G1	6.8	0.85	JONSWAP	3.3	–	–	50
G2	9.5	1.01	JONSWAP	3.3	–	–	50
G3	–	–	–	–	10	–	50
G4	–	–	–	–	20	–	50
G5	–	–	–	–	–	400	50
G6	–	–	–	–	–	500	50
G7	6.8	0.85	JONSWAP	3.3	10	–	50
G8	6.8	0.85	JONSWAP	3.3	20	–	50
G9	9.5	1.01	JONSWAP	3.3	10	–	50
G10	9.5	1.01	JONSWAP	3.3	20	–	50
G11	6.8	0.85	JONSWAP	3.3	–	400	50
G12	6.8	0.85	JONSWAP	3.3	–	500	50
G13	9.5	1.01	JONSWAP	3.3	–	400	50
G14	9.5	1.01	JONSWAP	3.3	–	500	50
G15	6.8	0.85	JONSWAP	3.3	10	400	50
G16	6.8	0.85	JONSWAP	3.3	10	500	50

Table 3. *Cont.*

Conditions	Random Wave				Steady Current	Uniform Wind	Water Depth (cm)
	H_s (cm)	T_s (s)	Wave Spectrum	γ_η	V_c (cm/s)	V_w (cm/s)	
G17	6.8	0.85	JONSWAP	3.3	20	400	50
G18	6.8	0.85	JONSWAP	3.3	20	500	50
G19	9.5	1.01	JONSWAP	3.3	10	400	50
G20	9.5	1.01	JONSWAP	3.3	10	500	50
G21	9.5	1.01	JONSWAP	3.3	20	400	50
G22	9.5	1.01	JONSWAP	3.3	20	500	50



Figure 4. Test scene of rigid model.

To ensure the accuracy of random wave simulation, the axial pumps were started first in the wave–current test conditions. When the water flow was stable, the wave generator was started. Similarly, the high-powered fan was started firstly in the wave–wind test conditions. When the wind speed was stable, the wave generator was started. In the wave–current–wind test conditions, the start sequence was high-powered fan, axial flow pumps, and then wave generator. According to the kinematic viscosity coefficient of water, model size, and test conditions, the Reynolds number in this test is in the automatic model area, which means that the relaxation of Reynolds criterion has little influence on the test results.

The test plans for elastic model were the same as the rigid model. The number of test conditions for elastic model is From E1 to E22. The test scene of elastic model is displayed in Figure 5.

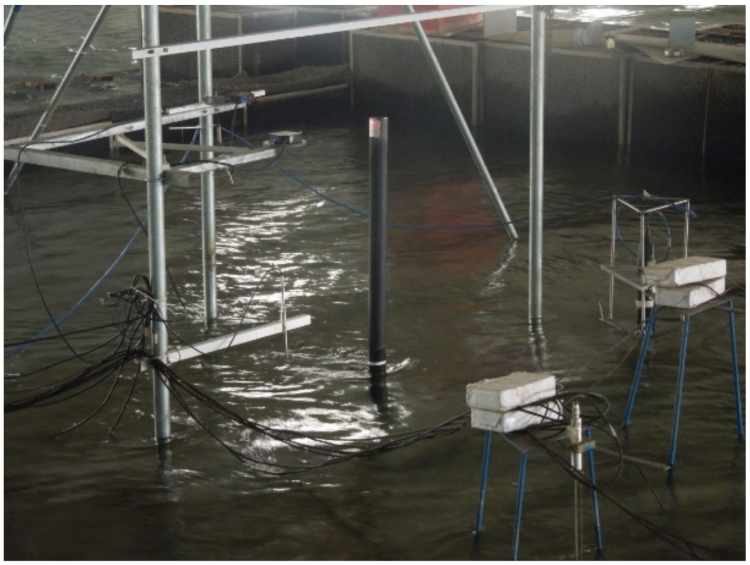


Figure 5. Test scene of elastic model.

3. Results and Discussion

3.1. Drag Forces of Rigid Model

Figure 6 displays the time histories and power spectrums of drag force (F_x) of rigid model under 4 different test conditions, i.e., conditions G1, G7, G11, and G15. It can be seen that $(F_x|\mathrm{G1}) < (F_x|\mathrm{G7}) < (F_x|\mathrm{G11}) < (F_x|\mathrm{G15})$, and the shapes of 4 drag force power spectrums are similar to the JONSWAP random wave spectrum. Their peak spectral frequencies were near 1.1 Hz, closely consistent with the peak spectral frequencies of incident random waves. The characteristics of drag forces in other conditions for rigid model are similar to Figure 6. This indicates that the frequency distribution of random wave cannot be changed by the combined action of steady current and uniform wind.

Figure 7 displays the characteristic values of drag forces of rigid model, where $F_{x,1\%}$ and $F_{x,s}$ represent the drag forces with non-exceedance probability of 1% and 13%, respectively, and $F_{x,mean}$ represents the mean value of F_x. As seen in Figure 7, whether significant wave height or mean wind speed or current velocity increase, the characteristic values will increase. The drag forces are affected most by significant wave height. Comparing the test conditions of G7~G10 with G1~G2 and G3~G4, it can be concluded that the characteristic values of combined action of wave and current are not the linear superposition of corresponding single field (single wave or current). Based on the test conditions of G1~G2, G5~G6, and G11~G14, a similar conclusion for wave and wind can also be reached. For the test conditions of combined action of wave, current, and wind (G15~G22), the characteristic values are more affected by current and wind when the significant wave height is smaller (H_s = 0.068 m). Obviously, the characteristic values of wave–current–wind are not the linear superposition of values of wave, current, and wind based on G1–G6 and G15–G22 ether. Furthermore, a certain extent of coupling effect exists when wave, current, and wind act together on the pile.

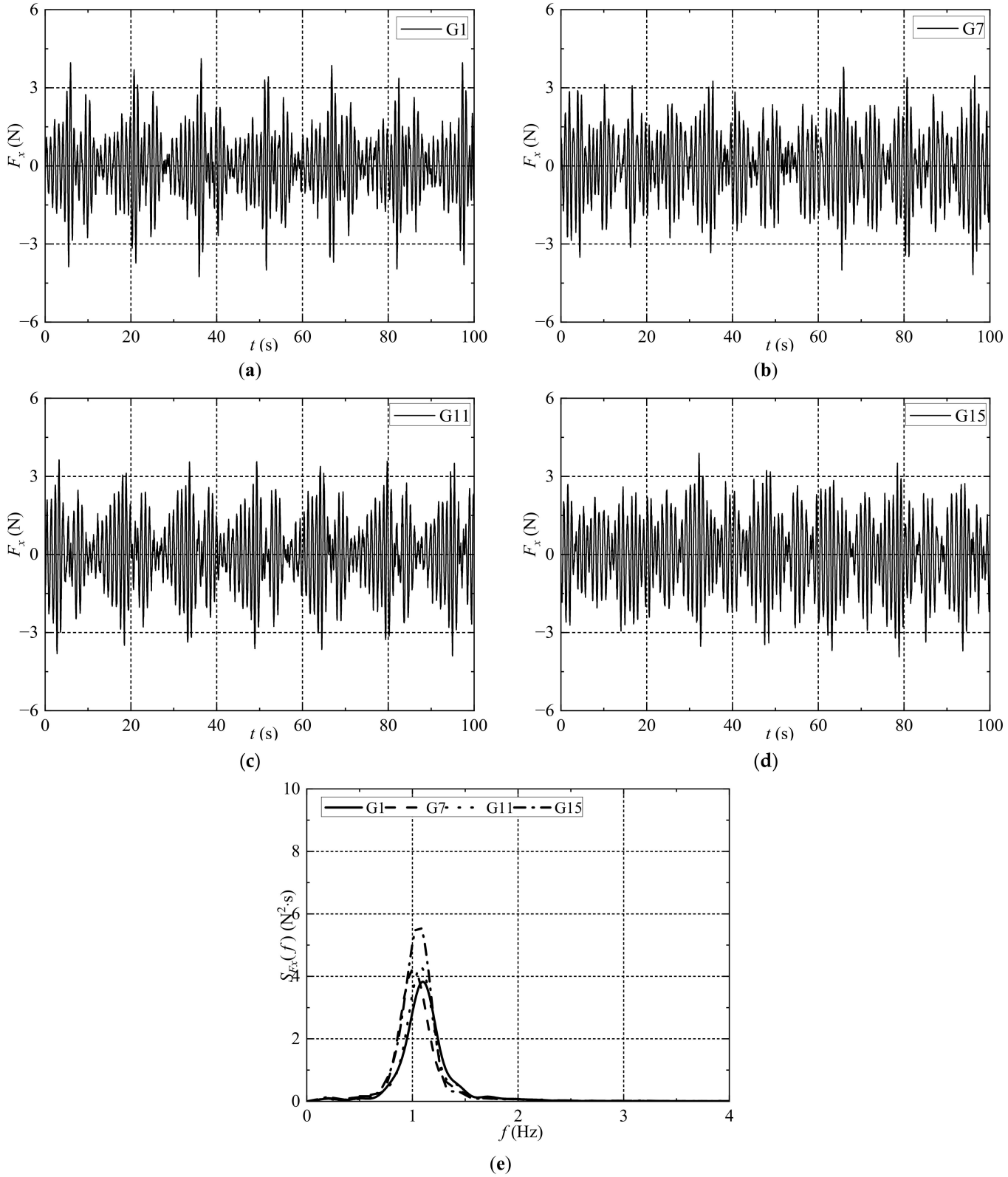


Figure 6. Time histories of drag force of rigid model for (**a**) G1, (**b**) G7, (**c**) G11, (**d**) G15, and (**e**) their power spectrums.

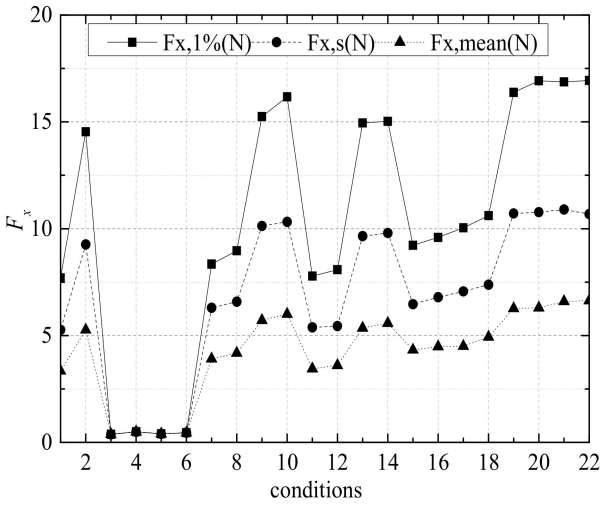


Figure 7. Characteristic values of drag forces of rigid model.

In order to quantitatively evaluate the coupling effects of wave–current, wave–wind, and wave–current–wind, two coupling coefficients are defined as follows:

$$\gamma_{i-j}^{n} = F_n / \left(F_i + F_j\right) - 1 \tag{1}$$

$$\gamma_{i-j-k}^{n} = F_n / \left(F_i + F_j + F_k\right) - 1 \tag{2}$$

In Equation (1), γ_{i-j}^{n} is the coupling coefficient for wave–current or wave–wind, n is the number of combined test condition, i is the number of wave condition and F_i is the corresponding characteristic value, j is the number of current or wind condition, and F_j is the corresponding characteristic value. In Equation (2), γ_{i-j-k}^{n} is the coupling coefficient for wave–current–wind, n is the same as Equation (1), i, j, and k are the test conditions of wave, wind, and current, respectively. F_i, F_j, and F_k are their corresponding values. According to the definition, the closer the γ_{i-j}^{n} and γ_{i-j-k}^{n} are to 0, the weaker the coupling effects are. If the coupling coefficient is greater than 0, the characteristic value of combined field is larger than the linear superposition of corresponding single field, which means that the coupling effect is unfavorable to marine structure. Conversely, if the coupling coefficient is smaller than 0, the characteristic value of combined field is smaller than the linear superposition of corresponding single field, which means that the coupling effect is favorable to marine structure.

Coupling coefficients of wave–wind, wave–current, and wave–current–wind for rigid model are displayed in Tables 4–6. It can be seen in Table 4 that for the combined action of wave and wind, the coupling coefficients are negative but close to 0, which means that the coupling effect of wave and wind is weak, and has a negligible influence on the characteristic value of wave–wind compared to the those of the corresponding single field. It is speculated that the weak wave–wind coupling effect may be because: (1) the interaction zone of wave and wind is near the water surface, which is far less than the height of the model, so that the influence of their interaction on the drag forces of rigid model is limited; (2) compared to wind, the contribution of wave on drag force is dominant, as its induced drag force is beyond 97.0%. In Table 4, the coupling coefficients of wave and current are positive but close to 0, which means that the coupling effect of wave and current is also weak. Compared to current, the contribution of wave is also dominant, as its induced drag force is beyond 85.5%. In Table 6, the coupling coefficients of wave–current–wind are also close to 0, which means the coupling effect among wave, wind, and current are weak. As shown in Tables 4–6, the increases of significant wave height, mean wind speed, and current velocity have little influence on the coupling effects.

Table 4. Coupling coefficients of wave–wind for rigid model.

Coefficient	$F_{x,1\%}$	$F_{x,s}$	$F_{x,\mathrm{mean}}$
γ^{11}_{1-5}	−0.065	−0.069	−0.079
γ^{12}_{1-6}	−0.044	−0.072	−0.051
γ^{13}_{2-5}	−0.013	−0.013	−0.055
γ^{14}_{2-6}	−0.017	−0.007	−0.025

Table 5. Coupling coefficients of wave–current for rigid model.

Coefficient	$F_{x,1\%}$	$F_{x,s}$	$F_{x,\mathrm{mean}}$
γ^{7}_{1-3}	0.007	0.095	0.051
γ^{8}_{1-4}	0.062	0.120	0.090
γ^{9}_{2-3}	0.009	0.039	0.012
γ^{10}_{2-4}	0.058	0.045	0.043

Table 6. Coupling coefficients of wave–current–wind for rigid model.

Coefficient	$F_{x,1\%}$	$F_{x,s}$	$F_{x,\mathrm{mean}}$
γ^{15}_{1-3-5}	0.036	0.032	0.050
γ^{16}_{1-3-6}	0.062	0.068	0.074
γ^{17}_{1-4-5}	0.108	0.106	0.063
γ^{18}_{1-4-6}	0.153	0.139	0.151
γ^{19}_{2-3-5}	0.041	0.044	0.038
γ^{20}_{2-3-6}	0.066	0.041	0.034
γ^{21}_{2-4-5}	0.061	0.049	0.070
γ^{22}_{2-4-6}	0.056	0.020	0.068

3.2. Drag Forces of Elastic Model

Figure 8 displays the time histories and power spectrums of drag forces of elastic model under wave, wave–current, wave–wind, and wave–current–wind, i.e., test conditions of E1, E7, E11, and E15. It can be seen that $(F_x|\mathrm{E1}) < (F_x|\mathrm{E7}) < (F_x|\mathrm{E11}) < (F_x|\mathrm{E15})$, which is the same with rigid model. However, the shapes of 4 drag force power spectrums are no longer similar to the JONSWAP random wave spectrum, as there are two peaks in the former. The first peak is at the frequency of 1.1 Hz, which is coincident with the peak spectral frequency of incident random wave. The second peak is at the frequency of 2.4 Hz, which is coincident with the first order frequency of the elastic model. The characteristics of drag forces in other conditions for elastic model are similar to Figure 8.

Figure 9 displays the characteristic values of drag forces for elastic model. The characteristic values of elastic model are close to those of the rigid model. This means that for the tested pile the natural vibration property has little influence on the drag forces. This is probably because the model's first order frequency (2.326 Hz) is far away from the peak spectral frequency (1.176 Hz) of incident wave, the elastic model could be seen as rigid, its vibration under wave, current, and wind is quite small, so that little interaction would happen between the model and flow field.

Tables 7–9 show the coupling coefficients of wave–wind, wave–current, and wave–current–wind for elastic model. The characteristics of coupling coefficients for the elastic model are quite similar to those for the rigid model (Tables 3–5), except that γ^{17}_{1-4-5} and γ^{18}_{1-4-6} reach about 0.12. However, in most cases, the coupling effects exist among three flow field are weak.

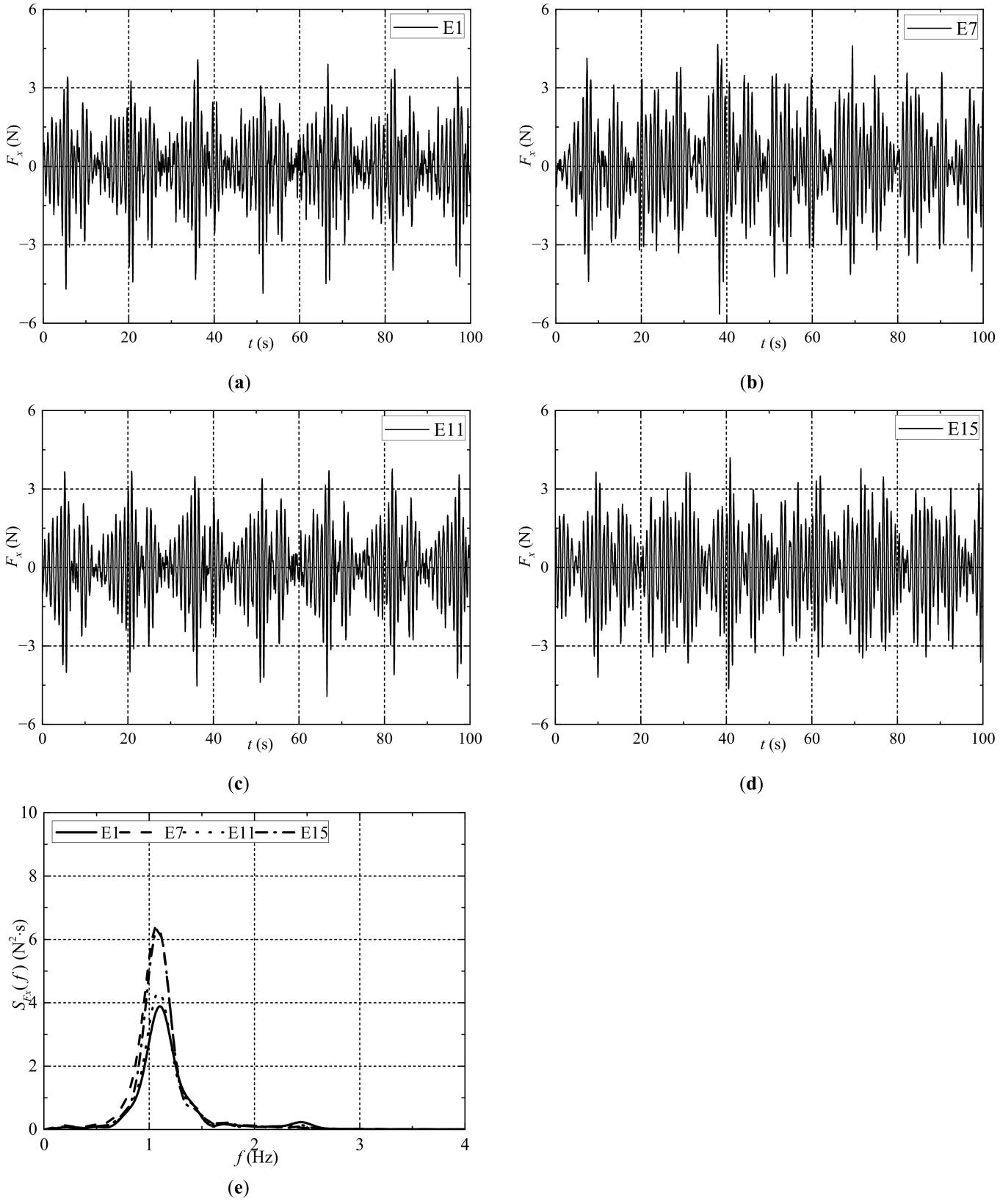


Figure 8. Time histories of drag force of elastic model for (**a**) E1, (**b**) E7, (**c**) E11, (**d**) E15, and (**e**) their power spectra.

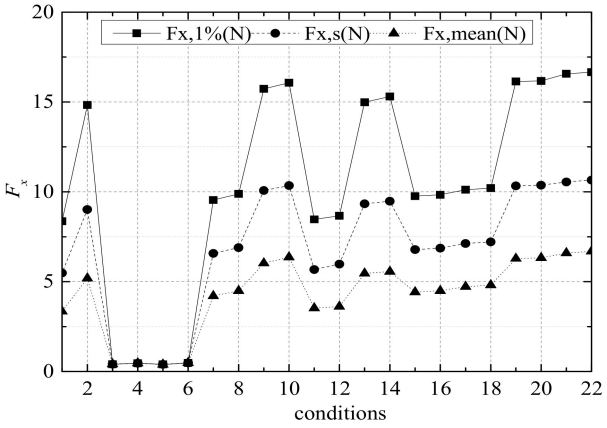


Figure 9. Characteristic values of drag forces of elastic model.

Table 7. Coupling coefficients of wave–wind for elastic model.

Coefficient	$F_{x,1\%}$	$F_{x,s}$	$F_{x,\mathrm{mean}}$/
γ_{1-5}^{11}	−0.060	−0.056	−0.058
γ_{1-6}^{12}	−0.051	−0.022	−0.055
γ_{2-5}^{13}	−0.032	−0.022	−0.020
γ_{2-6}^{14}	−0.019	−0.017	−0.017

Table 8. Coupling coefficients of wave–flow for elastic model.

Coefficient	$F_{x,1\%}$	$F_{x,s}$	$F_{x,\mathrm{mean}}$
γ_{1-3}^{7}	0.060	0.093	0.119
γ_{1-4}^{8}	0.065	0.120	0.177
γ_{2-3}^{9}	0.017	0.055	0.078
γ_{2-4}^{10}	0.021	0.068	0.128

Table 9. Coupling coefficients of wave–flow–wind for elastic model.

Coefficient	$F_{x,1\%}$	$F_{x,s}$	$F_{x,\mathrm{mean}}$
γ_{1-3-5}^{15}	0.011	0.038	0.064
γ_{1-3-6}^{16}	0.006	0.034	0.062
γ_{1-4-5}^{17}	0.019	0.067	0.122
γ_{1-4-6}^{18}	0.016	0.063	0.121
γ_{2-3-5}^{19}	0.001	0.027	0.051
γ_{2-3-6}^{20}	−0.004	0.020	0.043
γ_{2-4-5}^{21}	0.011	0.033	0.093
γ_{2-4-6}^{22}	0.009	0.033	0.094

4. Conclusions

The rigid and elastic models of a pile of a marine structure were tested in a harbor basin, and the coupling effects of wave–wind, wave–current, and wave–current–wind were investigated qualitatively and quantitatively. The main conclusions that can be drawn in this study are as follows.

1. The shape of power spectrum of drag force and the peak frequency are similar to the spectrum of incident wave, which agrees with the JONSWAP random wave spectrum. This means that the steady current and uniform wind cannot change the frequency distribution of incident random wave.
2. The drag forces of rigid and elastic model under wave–wind, wave–current, and wave–current–wind are not the linear superposition of corresponding single field, so that a certain extent of coupling effect exists among wave, flow and wind field.

3. Both in the rigid and the elastic model test, the coupling effects of wave–wind are weak. This may be because, firstly, the interaction zone of wave and wind is near the water surface, which is far less than the height of the model; secondly, the contribution of wave is dominant compared to wind. The coupling effects of wave–current and wave–current–wind are also weak. Therefore, in the structural design of a pile, the coupling effects among wave, current, and wind can be ignored.
4. The test results of elastic model are similar to the rigid model because the model's first order frequency is far away from the peak spectral frequency of the incident random wave, so that the natural vibration of the pile has little influence on the drag force. In this situation, the elastic model can be seen as rigid; the model's vibration under the action of wave, current, and wind is quite small so that little interaction between model and wave, current, and wind field will happen.

Author Contributions: Conceptualization, Z.T. and J.Y.; methodology, Z.T., J.Y., M.H. and W.L.; investigation, Z.T. and J.Y.; writing—original draft preparation, Z.T. and J.Y.; writing—review and editing, Z.T., J.Y. and M.H. All authors have read and agreed to the published version of the manuscript.

Funding: This research was funded by Zhejiang Provincial Natural Science Foundation of China (No. LGG22E080018, LQ19E080021).

Institutional Review Board Statement: Not applicable.

Informed Consent Statement: Not applicable.

Data Availability Statement: Not applicable.

Acknowledgments: The authors greatly appreciate the support by the Zhejiang Provincial Natural Science Foundation of China under Grant No. LGG22E080018 and LQ19E080021. The opinions and statements do not necessarily represent those of the sponsors.

Conflicts of Interest: The authors declare no conflict of interest.

References

1. Zhang, X. *Research on Sea-Crossing Bridge Main Pile Foundations Detection Evaluation Technology*; Xi'an University of Architecture and Technology: Xi'an, China, 2017.
2. Zhang, X.; Piao, L.; Fan, X.; Ye, X.; Li, C. Application of stainless-steel bar in durability design of cross-sea bridge. *J. Highw. Transp. Res. Dev.* **2017**, *S1*, 28–32.
3. Guo, G. Analysis on the reason of exposed steel bar of pile foundation of cross-sea bridge and its treatment and reinforcement scheme are introduced. *Fujian Jiaotong Technol.* **2018**, *3*, 23–28.
4. Zhou, D.; Xiao, S.; Du, F. Random Dynamic Response Analysis on Construction Platform Based on Wave Force. *J. Chongqing Jiaotong Univ. Nat. Sci.* **2008**, *27*, 370–373, 412.
5. Yu, S.; Ding, T. Bridge engineering splicing analysis. *J. Liaoning Tech. Univ. Nat. Sci.* **2010**, *29*, 47–48.
6. Huang, G.; Tian, L.; Zhao, X. Deformation prediction of bridge based on radial basis function neural network. *J. Liaoning Tech. Univ. Nat. Sci.* **2013**, *8*, 1103–1106.
7. Yang, N.; Zhu, X.; Qi, L.; Xiong, Y.; Wang, H. Design of distributed data acquisition system based on water tank of wind, wave and current. *Electron. Meas. Technol.* **2013**, *36*, 105–110.
8. Zou, Y.; Liu, L.; Wang, Y.; Luo, Z. Influence of Contact Surface on Dynamic Response of Bridge Pier Collided by Barge. *J. Chongqing Jiaotong Univ. Nat. Sci.* **2018**, *37*, 7–15.
9. Tu, Z.; Huang, M.; Lou, W. Extreme load effects on bridge tower-basement system due to joint actions of wind and wave. *J. Zhejiang Univ. Eng. Sci.* **2016**, *50*, 813–821.
10. Tu, Z.; Huang, M.; Lou, W. Extreme load effects on a bridge tower-basement system under the joint action of wind and wave based on the EC method. *J. Vib. Shock.* **2017**, *36*, 125–134.
11. Tu, Z.; Huang, M.; Lou, W.; Li, B. Dimensional environmental contour lines of the wind and wave based on Copula functions. *J. Vib. Shock.* **2021**, *40*, 1–9.
12. Sikirić, M.D.; Roland, A.; Janeković, I.; Kuzmić, M. Coupling of the Regional Ocean Modeling System (ROMS) and Wind Wave Model. *Ocean. Model.* **2013**, *8*, 59–73. [CrossRef]
13. Wei, S.-X.; Liang, Z.-D.; Cui, L.; Zhai, H.-L.; Jeng, D.-S. Numerical study of seabed response and liquefaction around a jacket support offshore wind turbine foundation under combined wave and current loading. *Water Sci. Eng.* **2022**, *15*, 78–88. [CrossRef]
14. Huang, Y.; Cheng, P.; Wan, D. Numerical Analysis of a Floating Offshore Wind Turbine by Coupled Aero-Hydrodynamic Simulation. *J. Mar. Sci. Appl.* **2019**, *18*, 82–92. [CrossRef]

15. Su, D. Discussion on experiment study method of wind-wave. *Ocean. Eng.* **1995**, *36*, 461–466.
16. Liu, J. *Research on the Dynamic Responses of a Freestanding Bridge Tower under the Coupling Action of Wind and Wave*; Harbin Institute of Technology: Harbin, China, 2015.
17. Chen, X. *Experiment on Viaduct Pier of Cross-Sea Bridge under Wind-Wave Action and the Wave Force Investigation*; Harbin Institute of Technology: Harbin, China, 2015.
18. Liu, N.; Li, B.; Wang, H.; Lv, H. A study of the influence of wave-current interaction on significant wave height in the Northwestern Pacific. *Acta Oceanol. Sinca* **2016**, *38*, 21–31.
19. Shang, D.; Wei, K.; Zhong, X.; Qin, S. Influence of wave-surge-current correlation on wave and current loads to elevated pile cap foundation of bridge under typhoons. *Eng. Mech.* **2022**, *39*, 187–194.
20. Fang, C.; Li, Y.; Xiang, H.; Zhang, J. Dynamic response influence of combined loads of wind, wave and current on sea-crossing bridges. *J. Southwest Jiaotong Univ.* **2019**, *54*, 908–914, 922.